Green Chemistry

PAPER

View Article Online
View Journal | View Issue

Cite this: *Green Chem.*, 2022, **24**, 8523

Aqueous conversion of monosaccharides to furans: were we wrong all along to use catalysts?†

Ana Jakob, [a,b] Blaž Likozar [*a,c,d] and Miha Grilc [*a,b]

Dehydration of the most relevant biomass derived monosaccharides, xylose, glucose and fructose, was investigated to attain value-added platform chemicals: furfural, hydroxymethylfurfural (5-HMF) and levulinic acid (LA). Reaction kinetics were studied in an aqueous environment in the presence and absence of the H-BEA zeolite. H-BEA demonstrated high activity, especially for isomerization of monosaccharides and rehydration of 5-HMF, while this work demonstrated that dehydration of sugars was governed predominantly by homogeneous reactions. Saccharide reactivity followed the trend of fructose > xylose > glucose, while 5-HMF was more susceptible to further conversion compared to furfural. The addition of H-BEA compromised 5-HMF yields (being an intermediate), and facilitated its further conversion to levulinic acid. The absence of a solid acid catalyst resulted in significant amounts of furfural and 5-HMF, whereas the addition of H-BEA resulted in higher yields of levulinic acid (26 mol% and 30 mol%). Excellent agreement between experimental and modelled values allowed the use of kinetic parameters for predictive modelling and optimization of the process conditions for maximizing the yields of 5-HMF and LA. The optimization was experimentally validated, where homogeneously catalyzed dehydration of fructose resulted in the highest 5-HMF yield (52 mol%) attained in 34 min at 234 °C due to the high activation energy (139 kJ mol^{-1}) and reaction rate constants. In contrast, the highest LA yield was achieved at moderate operational temperatures (165 °C) and longer reaction times (10 h) as a result of a significantly lower energy barrier (60 kJ mol^{-1}) determined for rehydration reactions.

Received 22nd July 2022,
Accepted 5th October 2022

DOI: 10.1039/d2gc02736d

rsc.li/greenchem

Introduction

The world's persistent increase in energy demand and continuous exploitation of fossil fuels have increased the urge to seek for alternative resources in order to lower the environmental burden caused by increased greenhouse gas emissions. With an estimated yearly production of more than 170 billion tonnes, lignocellulosic biomass, the most abundant sustainable feedstock, offers a massive capacity of renewable carbon resources.[1] Efficient conversion of saccharide-rich biomass fractions, namely cellulose and hemicellulose, can be predominantly applied for the production of bio-based compounds such as hydroxymethylfurfural (5-HMF), furfural and levulinic acid (LA). All three of these compounds can be further converted into valuable platform chemicals that can serve as various precursors and are especially significant in the polymer industries namely adhesives, coatings and resins.[2–10] Prior to the catalytic conversion of biomass derived saccharides, acquired hemicellulose and/or cellulose fractions are generally subjected to acid hydrolysis in order to obtain their respective monosaccharides, xylose and glucose. Subsequently, the attained glucose and xylose can serve as substrates for the dehydration reaction towards 5-HMF/LA and furfural, respectively.[11–13] Despite glucose being a low cost and widely available saccharide feedstock, its conversion towards 5-HMF and LA is much more challenging compared to its isomer fructose.[14] For this reason, we aim to investigate the conversion of three of the most relevant biomass-derived saccharides under different operating conditions. Regardless of all the efforts and increasing research in the field of biomass, particularly saccharides, conversion in aqueous media at elevated temperatures remains problematic due to the compromised saccharide and furanic (5-HMF and furfural) stability.[15–17] Consequently, dehydration generally results in significant amounts of complex polymeric degradation products commonly referred to as humins.[15,18,19] Humins formation greatly lowers product selectivity, plausibly by pore clogging and/or catalyst deactivation leading to overall process inefficiency.[20,21] Despite all of the current challenges, water as a solvent offers an environmentally friendly, non-toxic alternative in comparison with

[a]*Department of Catalysis and Chemical Reaction Engineering, National Institute of Chemistry, Hajdrihova 19, 1000 Ljubljana, Slovenia. E-mail: miha.grilc@ki.si*
[b]*University of Nova Gorica, Vipavska 13, 5000 Nova Gorica, Slovenia*
[c]*Pulp and Paper Institute, Bogišićeva 8, 1000 Ljubljana, Slovenia*
[d]*Faculty of Polymer Technology, Ozare 19, 2380 Slovenj Gradec, Slovenia*
† Electronic supplementary information (ESI) available. See DOI: https://doi.org/10.1039/d2gc02736d

organic solvents (THF, DMSO, DMF, MTHF, *etc*.). To improve the process efficiency and yields of either furanics or LA, mineral acids such as HCl and H_2SO_4 are commonly used as homogeneous acid catalysts for C6 and C5 sugar dehydration. Dilute H_2SO_4 has also been used in one of the commercialized lignocellulosic fractionation technologies, the Biofine process.[22] Despite providing superior performance, homogeneous catalysts pose a high environmental risk due to their corrosive properties. Alternatively, heterogeneous solid acids such as zeolites, hetero-polyacids, and ion exchange resins offer much easier separation and therefore, are often a more desired choice for a catalyst, especially on the industrial scale.[23–25] Aiming towards sustainable and environmentally friendly processes, we focused on the use of the H-BEA zeolite as a heterogeneous catalyst for the production of 5-HMF/LA and furfural. Zeolites offer a vast number of possibilities for biomass conversion, and can be used for acid catalysed dehydration, or doped and further used for various other reaction routes.[26–29]

To overcome all of the aforementioned challenges and make heterogeneous catalyst utilization more efficient, it is necessary to gain an enhanced understanding of the saccharide dehydration process which can be elucidated by the application of kinetic studies. This approach can be particularly valuable for process optimization and rational catalyst design. Until now, different modelling approaches have been used to study reaction kinetics and are summarized in Table 1. Simple macro-kinetic models, using a power-law approach, have been extensively adopted to describe the reaction kinetics of especially homogeneously catalysed reactions.[30,35] On the other hand, the experimental data of saccharide dehydration usually follow a first order reaction mechanism and therefore, authors commonly use first order kinetics to describe saccharide conversion.[31,34] Reactions occurring without a catalyst in pure solvent (blank reaction) are frequently not reported in existing kinetic studies of saccharide conversion or are considered insignificant under the selected reaction conditions. Consequently, the role of the catalyst is often not presented independently of external factors that are possibly influencing the reaction kinetics.

Interestingly, most studies of saccharide conversion are often focused on only one particular saccharide, and do not always include the information of their respective isomers. The pathway of saccharide conversion is known to be strongly

Table 1 Kinetic studies of saccharide (xylose, glucose, and fructose) dehydration over

Feedstock	T [°C]	Catalyst	Kinetic model	Yields of furfural/ LA/5-HMF	Reaction network	Ref.
Fructose	140–180	H_2SO_4	Power-law modeling	74 mol% (LA) 53 mol% (5-HMF)	Fructose → 5-HMF 5-HMF → LA + FA Fructose → humins 5-HMF → humins	30
Glucose	180–220	High-temperature liquid water	First order kinetic model	32% (5-HMF)	Glucose → 5-HMF 5-HMF → LA Glucose → humins 5-HMF → humins LA → degradation products	31
Glucose	130–190	HY-zeolite	First order kinetic model	—	Glucose → 5-HMF Fructose → 5-HMF 5-HMF → LA + formic aicd Glucose ↔ fructose	28
Glucose	160–200	HZSM-5 8% Cr/HZSM-5	Pseudo first-order model	23% (LA) 64% (LA)	Glucose → 5-HMF 5-HMF → LA + formic acid	32
Xylose	140–220	HZSM-5 zeolite	First order kinetic model	46% (furfural)	Xylose ↔ lyxose Lyxose → furfural Xylose → furfural Furfural → formic acid Furfural → furilic species Formic acid → furilic species Furilic species → furfural	29
Xylose	170	Nanocrystalline zeolite beta	Pseudo-homogeneous kinetic model	77% (furfural)	Xylose → intermediate Intermediate → furfural Intermediate → pentose degradation product Xylose → pentose degradation product Furfural → pseudo-unimolecular degradation product Furfural → degradation product	33
Xylose	180–220	High-temperature liquid water	First order kinetic model	50% (furfural)	Xylose → furfural Furfural → degradation products Xylose → degradation products	34

LA; levulinic acid, FA; formic acid.

affected by the selected solvent and the type of catalyst. Despite the known reaction mechanisms and regardless of the catalyst properties, kinetic models can differ significantly due to the required model simplification and/or variations in the reaction system and conditions. Although the applications of heterogeneous catalysts have been excessively studied in the literature, kinetic studies that include catalyst surface reactions are rather scarce. Kinetic studies of glucose and xylose dehydration over a solid acid catalyst conducted by Lourvanij *et al.* and O'Neill *et al.* are two of the few studies covering a complex reaction mechanism, including the saccharide isomerization reaction and catalyst surface reactions related to desorption and adsorption.[28,29] Therefore, the aim of this paper was to develop an extensive kinetic model for both homogeneously (in the absence of a catalyst) and heterogeneously catalysed glucose/fructose and xylose dehydration under hydrothermal conditions. This enabled the comparison among the reactivity of hexoses (fructose, glucose) and pentoses as well as the investigation of differences in the conversion of their respective saccharide forms: aldoses (glucose, xylose) and ketoses (fructose).

Experimental methods

Materials

Glucose (Merck, ≥99%), fructose (Merck, ≥99%) and xylose (SAFC®, ≥99%) were used as substrates for the dehydration reactions. Calibration standards for product quantification were prepared using glucose (Merck, ≥99%), fructose (Merck, ≥99%), xylose (SAFC®, ≥99%), D-(−)-lyxose, furfural (Sigma Aldrich, 99%), hydroxymethylfurfural (Sigma Aldrich, 99%), levulinic acid (Sigma Aldrich, 98%), and formic acid (100%, Merck). Commercially purchased H-BEA zeolite (SiO_2/Al_2O_3 = 28, Tosoh Corporation) was used as a catalyst and Milli-Q water was used for reaction solution preparation. Sulphuric acid (Merck, 95–97%) was used to prepare 5 mM mobile phase solution. 10 bars of N_2 supplied from 5.0 Messer (Bad Soden am Taunas, Germany) was used as an inert atmosphere for dehydration experiments.

Analytical methods

External standards of saccharides (glucose, fructose, xylose, lyxose), acids (formic and levulinic acid) and furanics (hydroxymethylfurfural and furfural) were used for reaction substrates, product identification, and preparation of calibration solutions. Quantification was carried out *via* ultra-high pressure liquid chromatography (UHPLC–DAD/RI, Ultimate 3000, Thermo Scientific) using a Rezex RHM monosaccharide H^+ column. The operation temperature of the column was set to 60 °C with a post column temperature of 30 °C. A solution of sulphuric acid with 5 mM concentration was used as a mobile phase at a flow rate of 0.6 mL min^{-1} and the time of each run was set to 60 min. The present saccharides and acids were quantified as a function of time using a refractive index detector, with the constant temperature set at 35 °C. Due to the similar response of C5 saccharides, lyxose was selected as the standard to determine intermediate (xylulose/lyxose) concentrations reported in ESI Fig. 19†.[36] Additionally, a diode array detector (DAD) was used for the quantification of furanics, where two respective wavelengths of 284 nm and 274 nm were used to monitor 5-HMF and furfural. Finally, the size of the insoluble residue (humins) was determined using size-exclusion chromatography (SEC). The analysis was performed on UHPLC–DAD/RI, Ultimate 3000 (Thermo Scientific), using polystyrene standards, following the analytical method described elsewhere with slight modifications.[19]

Monosaccharide conversion

Sugar dehydration reactions were conducted in six, stainless steel, 75 mL (Parr) batch reactors, equipped with online pressure and temperature control regulators. The reaction mixture was stirred using a magnetic stirring bar with a stirring speed of 600 rpm. A precise amount (500 mg) of individual saccharides (glucose, fructose and xylose) was introduced into each reactor vessel. For the heterogeneously catalysed reaction, 500 mg of H-BEA zeolite was added into the reactor vessel. Water was then added as a solvent to make up to a total weight of 50 grams. Prior to the start of the reaction, reactors were purged three times with N_2 and all catalytic activity tests were conducted under an inert atmosphere under 10 bars of N_2. Dehydration reactions were performed for 5 h once the set reaction temperature was reached, with a heating ramp of 5 °C min^{-1}. The influence of temperature on the catalytic activity and product distribution was studied in the range of 130–190 °C. During the reaction, samples were collected every 45 min, *via* a sampling line, to study the kinetics of sugar conversion and product formation as a function of time. Prior to the analysis, all collected samples were filtered through cellulose acetate filters. Samples were analysed offline by ultra high performance liquid chromatography (UHPLC–DAD/RI, Ultimate 3000, Thermo Scientific).

Catalyst characterization

The acid properties of the catalyst were measured by temperature programmed desorption of ammonia (NH_3-TPD), using Micrometrics AutoChem II. Analysis was conducted by precisely weighing 0.1 g in a U-shaped quartz tube. Prior to the measurement, the catalyst sample was flushed with He for 60 min at 500 °C to remove all residual moisture possibly trapped in the pores. As the sample cooled down to 100 °C, NH_3 was adsorbed to the catalyst surface by saturating the system with 10 vol% NH_3 in He for 30 min, with a flow rate of 20 mL min^{-1}. This was followed by sample purging for 60 min at 100 °C using He. The data were collected when the temperature increased from 100 °C to 700 °C, with a heating ramp of 10 °C min^{-1} and He as a carrier gas. For the quantification of desorbed NH_3, a thermal conductivity detector (TCD) equipped with a quadrupole mass spectrometer was used. The spectra of m/z = 15, representing NH_3, were observed to quantify the number of acid sites on the surface of the H-BEA zeolite.

Catalyst stability was tested by three different methods and are depicted in ESI Fig. 4–6.† The possibility of carbon deposits present on the spent catalyst surface was quantified by total organic carbon (TOC) analysis, using Rosemount Dohrmann Apollo. The crystalline structure of the fresh, spent and regenerated catalyst was studied by X-ray diffraction (XRD) analysis. Patterns in the 2θ range from 5° to 80° using Cu Kα as a radiation source (λ = 1.54056 Å) were collected using an X'Pert PRO MPD instrument. The morphology of the fresh, spent and regenerated catalyst was characterized using field emission scanning electron microscopy (FE-SEM, SUPRA 35-F, Carl Zeiss).

Formulas for the yield and selectivity calculation

In order to calculate the conversion (X_j) and yields (Y_j) of a compound (j), the following equations were used:

$$X_j(t) = \frac{c_{j(0)} - c_{j(t)}}{c_{j(0)}} \times 100 \quad (1)$$

$$Y_j(t) = \frac{c_{j(t)}}{c_{\text{reactan }t(0)}} \times 100 \quad (2)$$

Eqn (1) refers to the conversion (X_j) of a reactant xylose, fructose or glucose, where $c_j(0)$ and $c_j(t)$ represent the starting concentration and concentration collected at time t. In eqn (2), $c_j(t)$ represents the concentration of a compound j (furfural, 5-HMF and LA) quantified in liquid samples taken at time t.

Kinetic model development

Kinetic model development in aqueous media without a catalyst. Based on the existing literature and products quantified during xylose and glucose/fructose conversion, a reaction pathway for each saccharide was developed, which is shown in Fig. 1 and 4, respectively.[4,18,37]

According to the reaction scheme, the reaction rates (eqn (3)) were proposed to be of first order, where a reaction rate of a homogeneous reaction (r_i^{homo}) depends only on the reaction rate constant and the concentration of the corresponding reactant in the reaction scheme. A set of molar balances was written as an ordinary differential in eqn (3a) which was solved numerically in Matlab 2018 using the Runge–Kutta 2–3 method. The influence of temperature on the reaction rate constants was calculated using Arrhenius law demonstrated in eqn (4).

$$r_i^{\text{homo}} = k_i C_j \quad (3)$$

$$\frac{dC_j^{\text{L}}}{dt} = \sum \pm r_i^{\text{hom o}} \quad (3a)$$

$$k_i(T_2) = k_i(T_1) \times \exp\left(\frac{E_{ai}}{R}\left(\frac{1}{T_1} - \frac{1}{T_2}\right)\right). \quad (4)$$

Kinetic model development in aqueous media with a heterogeneous catalyst. A comprehensive kinetic model was developed based on the proposed reaction schemes for both C5 (xylose) and C6 (glucose/fructose) dehydration. Mechanism 2 (heterogeneous xylose dehydration) in Fig. 1 and Mechanism 4 (heterogeneous fructose/glucose dehydration) in Fig. 4 demonstrate the reaction steps occurring on the catalyst surface in aqueous media at the temperature range of 130–190 °C. As mentioned above, reaction mechanisms were developed based on the reported literature and liquid products identified during the xylose, glucose and fructose dehydration reactions.[29,33,37,38]

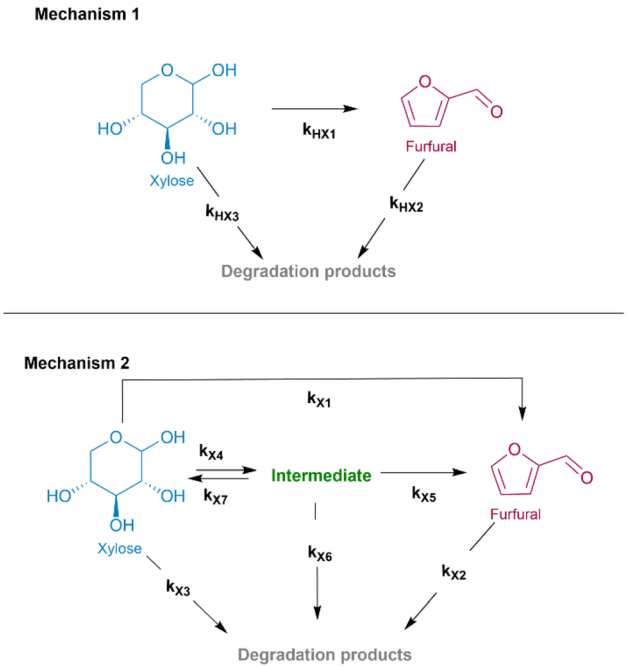

Fig. 1 Homogeneously (mechanism 1) and heterogeneously (mechanism 2) catalysed dehydration of xylose.

The established kinetic model was based on a set of ordinary differential equations, considering the concentration of compounds detected in the liquid phase and their coverage on the catalyst surface. For the sake of simplicity, the developed kinetic model follows the following assumptions:

- The reaction rate of desorption was assumed to be faster in comparison with the rate of adsorption.
- Due to model simplification and structural similarities between compounds, adsorption and desorption constants were unified for all detected species, and are according to the study reported by Šivec *et al.* significantly higher compared to the reaction rate constant.[39] Therefore, adsorption and desorption constants do not represent the rate limiting step of the studied reaction.
- Degradation product formation followed 1st order kinetics and due to the difficulties in their quantification, the amount of degradation products was calculated considering the remaining unaccounted carbon balance, according to the studies conducted by Bounoukta and Kojčinović *et al.*[40,41]
- The active sites on the catalyst surface were assumed to equal the concentration of acid sites within the mesoporous area of the catalyst, measured by NH_3-TPD and BET methods.[25] Furthermore, it was assumed that a single molecule covers one acid site.

• All existing vacant active sites were considered equal and independent for overall coverage as the reaction proceeds.

• All the homogeneous and heterogeneous reaction steps occur simultaneously and independent of each other. This was confirmed by the experiments conducted with and without a catalyst, where plausible homogeneous H-BEA catalytic activity was tested by hot and cold filtration experiments and is demonstrated in the ESI Fig. 6.†

• Prior to the calculation of heterogeneous kinetic parameters, homogeneously catalyzed reactions were fitted separately and parameters were later held constant when determining heterogeneous kinetics.

For reactions on the catalyst surface, we assumed that the adsorption rate r_j^{ads} equals the reaction rate constant of adsorption k_j^{ads} for each compound, its concentration in the liquid phase C_j^L and concentration of vacant sites θ_{VS}.

$$r_j^{ads} = k_j^{ads} C_j^L \theta_{VS} \quad (5)$$

The desorption rate r_j^{des} is determined by the desorption reaction rate constant of compound j, k_j^{des} and its coverage θ_j in addition to the reaction rate of the homogeneous reactions of individual compounds.

$$r_j^{des} = k_j^{des} \theta_j \quad (6)$$

The surface rate r_i^{surf} of a reaction (i) depends on the surface rate constant (k_i), being temperature-dependent as per eqn (4), and the surface coverage of the corresponding reactant (θ_j).

$$r_i^{surf} = k_i \theta_j \quad (7)$$

The overall balance of compounds in the liquid phase can be described by the equation below, where n_{TS} represents the number of total sites and V represents the total volume of the reaction solution and the sum of the reaction rates of homogeneous reactions of each compound r_j^{homo}. The total concentration of active sites was determined experimentally by NH_3-TPD and BET, ascribed to the mesoporous acidity of the selected catalyst.

$$\frac{dC_j^L}{dt} = -r_j^{ads} + r_j^{des}\frac{n_{TS}}{V} + \sum_i^I \pm r_i^{homo}. \quad (8)$$

For the mathematical description of the balance on the catalyst surface, we used the following equation (eqn (9)) where all compounds consumed or/and formed from compound j are described with parameter i.

$$\frac{d\theta_j}{dt} = r_j^{ads}\frac{V}{n_{TS}} - r_j^{des} + \sum_i^I \pm r_i^{surf}\frac{1}{n_{TS}}. \quad (9)$$

In the case of stoichiometrically unbalanced reactions, the correction of vacant active site coverage can be implemented by the use of eqn (10).

$$\frac{d\theta_{vs}}{dt} = \left(-V\sum_j^J r_j^{ads} + \sum_j^J r_j^{des} + \sum_i^I \pm r_i^{surf}\right)\frac{1}{n_{TS}} \quad (10)$$

$$f(k_{i-j}, E_{ai-j}) = \sum_{exp=1}^{EXP}\sum_{j=1}^{J}\left(C_{j\,exp}{}^L - C_{j\,mod}{}^L(k_{i-j}, E_{ai-j})\right)^2. \quad (11)$$

As a regression method, the Nelder–Mead method, described by eqn (11) was used to minimize the objective function, while additionally the Levenberg–Marquardt method was applied to obtain a Jacobian matrix and 95% confidence intervals.

Results and discussion

Catalyst characterization (scanning electron microscopy, acidity NH_3-TPD and pyridine DRIFT)

Scanning electron microscopy (SEM) was used to investigate the morphology of the H-BEA zeolite. Spherical shaped particles, typical of the H-BEA type of zeolite, with the size of 200–400 nm can be observed in ESI Fig. 4.†[42] According to the analysis of the structural properties, which was previously conducted by our group, the H-BEA (28) catalyst demonstrated a surface area of 549 $m^2\ g^{-1}$, with a total pore volume of 0.32 $cm^3\ g^{-1}$, and an average crystallite size of 16.7 nm.[42] In addition, the catalyst crystallinity was investigated by X-ray diffraction analysis, which verified the typical pattern for the H-BEA zeolite at 22.5, 21.4 and 7.8°, in the 2θ region (ESI, Fig. 5†). The total density of acid sites of the catalyst was determined by temperature programmed NH_3 desorption, with the value of 1.1 mmol of NH_3 per g. As presented in the ESI Fig. 3,† two peaks of weak and strong acid sites were detected and quantified by Gauss deconvolution. According to the previously conducted study by our group by Kostyniu *et al.*, pyridine-DRIFTS analyses of H-BEA (28) catalyst demonstrated the presence of both Lewis and Brønsted acid sites with a B/L ratio of 1.2.[42] Brønsted acid sites in the H-BEA zeolite originate from the bridging of Al^{4+} and the silanol group (Si–OH–Al), while the external-framework of Al-oxide and/or octahedral Al atoms are usually the source of Lewis acidity.[43–47] The acid properties of the H-BEA zeolite are summarized below in Table 2.

Saccharide dehydration in HLW

Mechanism of xylose dehydration

Mechanism 1 depicted in Fig. 1 describes xylose dehydration in aqueous media at elevated temperatures in the absence of the solid catalyst (H-BEA zeolite). In this case, xylose is dominantly converted into furfural *via* direct dehydration (k_{HX1}); furthermore, two steps of xylose (k_{HX3}) and furfural degradation (k_{HX2}), were added since both xylose and furfural appear to degrade into smaller fractions, such as organic acids, formaldehyde, *etc*. and/or polymerize towards insoluble humin species.[18,48] To experimentally confirm the degradation of xylose and furfural, furfural degradation was studied separately at three different temperatures (130, 160 and 190 °C) and is presented in ESI Fig. 8.† SEC analysis of xylose derived insoluble humins formed during hydrothermal treatment at

Table 2 Acid properties of the H-BEA (28) zeolite

	Acidity by NH_3-TPD (mmol NH_3 per g_{cat})					Acidity by Pyr-DRIFTS[a] (%)		
Catalyst	Total	Weak	T (°C)	Strong	T (°C)	C_{BAS}	C_{LAS}	B/L ratio
H-BEA (28)	1.1	0.43	201	0.67	324	54.9	45.1	1.2

[a] Pyr-DRIFT analysis were taken from ref. 42.

175 °C also identified larger molecular species with a molecular weight ranging from 150 Da up to 3000 Da, as shown in ESI Fig. 7.† This phenomenon of excessive humin formation is particularly pronounced in aqueous environments. Nevertheless, hydrothermal treatment with or without the addition of a catalyst is a commonly used approach for saccharide conversion. Particularly, experiments conducted under hydrothermal conditions in the absence of a catalyst demonstrated significant furfural yields obtained in the temperature range of 130–190 °C, especially when the reaction temperature was increased above 145 °C (ESI Fig. 9†). In water at the elevated temperatures, or so called subcritical water (100–374 °C), the concentration of H_3O^+ and OH^- ions increases.[12,25] Subsequently, this enables the aqueous media to act as a catalyst.[49–51]

When studying xylose dehydration over the H-BEA zeolite, the nature of the catalyst (the presence of Lewis acidity) specifically effected the reaction pathway (Mechanism 2, Fig. 1). Due to the introduction of strong Lewis acidity, the conversion of xylose proceeded *via* an additional isomerization step. Therefore, the reaction scheme for xylose dehydration of H-BEA was extended by two reversible isomerization reaction steps (k_{X4} and k_{X7}). Similar to the reactions conducted in aqueous media without a catalyst, humin and side product formation became unavoidable when using a solid acid catalyst (H-BEA). Three possible pathways of humin formation were included in our model, which were validated by other kinetic studies.[29,33,34] Thus, the reaction rate constants k_{X2}, k_{X3} and k_{X6} represent the degradation of furfural, xylose, and the intermediate, respectively. Kinetic parameters of furfural degradation over the H-BEA zeolite were additionally experimentally confirmed and are presented in the ESI Fig. 12.†

Overall, two of the proposed reaction mechanisms of xylose dehydration in the absence (Mechanism 1) and presence (Mechanism 2) of the H-BEA zeolite differ in the xylose isomerization step. Due to the absence of strong Lewis acidity, isomerization towards intermediates was not detected. Mechanistically, the role of Brønsted and Lewis acid catalytic activity was elucidated by Choudhary *et al.*, where Brønsted acidity promotes direct xylose dehydration,[52] whereas the presence of Lewis acidity facilitates xylose isomerization *via* intramolecular hydride-transfer.[18,53] Based on the literature, the detected intermediates can be one of the two compounds, either xylulose or lyxose, respectively.[36,53]

Kinetics of xylose dehydration in HLW

Reactions of xylose dehydration under hydrothermal operational conditions were conducted in aqueous media without a catalyst in the temperature range of 130–190 °C starting with 1 wt% xylose concentration. The highest reaction temperature of 190 °C yielded 45 mol% furfural after 165 min, demonstrating the highest yield recorded in the absence of the catalyst within the studied temperature range. Temperature had a significant influence on the xylose conversion as well as furfural and humin formation. Based on the calculated kinetic parameters, it was confirmed that xylose dehydration to furfural occurs the fastest with the highest calculated reaction rate constant (k_{HX1}) of 1.11×10^{-3} min^{-1} and E_a of 122 kJ mol^{-1}.

Furfural-derived humin formation (k_{HX2}) appears to not be as significantly influenced by reaction temperature, with a calculated E_a of 71 kJ mol^{-1}, while formation of xylose-derived humin formation (k_{HX3}) tends to be considerably more pronounced at elevated temperatures (E_a 213 kJ mol^{-1}). However, xylose-derived humin formation was remarkably slower (~50%) compared to furfural degradation to humins. Increased reaction temperatures consequentially resulted in increased yields of furfural; however, that also simultaneously decreased its selectivity due to the pronounced degradation of both xylose and furfural. The concentration profile of xylose and furfural during the dehydration reaction at 160 °C is depicted in Fig. 2. While the overall influence of temperature on the xylose conversion and product distribution throughout the reaction is depicted in ESI Fig. 9.† Calculated kinetic parameters are summarized in Table 3. Jing *et al.* studied the kinetics of xylose degradation at slightly higher temperatures

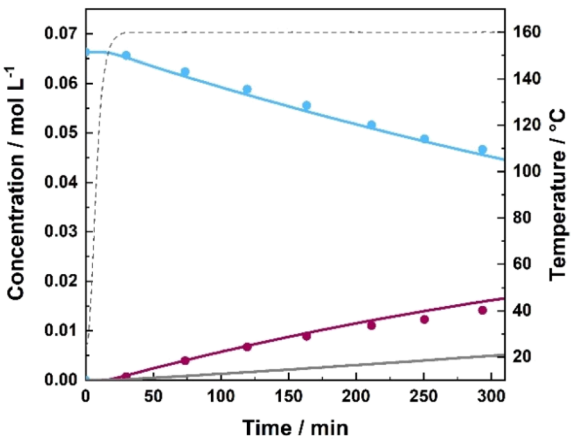

Fig. 2 The product distribution as a function of the time for the xylose dehydration reaction in aqueous media without H-BEA at 160 °C, where symbols represent experimental points and lines correspond to model values • xylose, • intermediate • furfural, – humins, ----- temperature.

Table 3 Calculated kinetic parameters for xylose, glucose and fructose dehydration under hydrothermal conditions with and without catalyst

i	Reaction rate constants at 160 °C, k_i[min^{-1}]	Activation energies, E_{ai}[kJ mol^{-1}]	i	Reaction rate constants at 160 °C, k_i[min^{-1}]	Activation energies, E_{ai}[kJ mol^{-1}]
1_{HX}	$(1.11 \pm 0.05) \times 10^{-3}$	122 ± 2	1_X	$(9 \pm 6) \times 10^{-5}$	30 ± 3
2_{HX}	$(5.68 \pm 2.0) \times 10^{-4}$	71 ± 11	2_X	$(9 \pm 3) \times 10^{-5}$	31 ± 5
3_{HX}	$(2.23 \pm 0.3) \times 10^{-4}$	213 ± 4	3_X	$(3.1 \pm 1.1) \times 10^{-5}$	41 ± 7
			4_X	$(8.4 \pm 0.3) \times 10^{-1}$	116 ± 5
			5_X	$(6.4 \pm 0.6) \times 10^{-1}$	99 ± 5
			6_X	$(9.7 \pm 0.8) \times 10^{-1}$	105 ± 4
			7_X	$<6.97 \times 10^{-6}$	95 ± 4
1_{HG}	$(3.18 \pm 0.13) \times 10^{-3}$	139 ± 6	1_G	$(2.46 \pm 0.78) \times 10^{-4}$	10 ± 1
2_{HG}	$(4.86 \pm 0.95) \times 10^{-4}$	98 ± 7	2_G	$(1.76 \pm 0.27) \times 10^{-1}$	151 ± 8
3_{HG}	$(1.36 \pm 0.1) \times 10^{-3}$	106 ± 7	3_G	$(3.83 \pm 0.68) \times 10^{-1}$	140 ± 7
4_{HG}	$(4.21 \pm 1.35) \times 10^{-4}$	108 ± 10	4_G	$(2.39 \pm 0.16) \times 10^{-1}$	136 ± 8
5_{HG}	$(4.49 \pm 0.80) \times 10^{-4}$	120 ± 9	5_G	$(2.83 \pm 0.16) \times 10^{-1}$	97 ± 7
6_{HG}	$< 1.6 \times 10^{-6}$	78 ± 10	6_G	$(1.83 \pm 0.89) \times 10^{-4}$	21 ± 2
7_{HG}	$(6.32 \pm 0.87) \times 10^{-4}$	85 ± 5	7_G	$(1.25 \pm 0.58) \times 10^{-4}$	17 ± 7
			8_G	$(8.68 \pm 1.01) \times 10^{-1}$	60 ± 7

(180–220 °C) and demonstrated comparable results where they obtained a maximum furfural yield of 50 mol%.[12,34] Correspondingly, Jing *et al.* estimated xylose dehydration to furfural to proceed the fastest, whereas its conversion into degradation products had the highest E_a of (143 kJ mol^{-1}), followed by xylose to furfural dehydration (112 kJ mol–1) and furfural-derived humin formation (59 kJ mol^{-1}).[34] Nabarlatz *et al.* reported an activation energy of 123 kJ mol^{-1} for xylose dehydration and 132 kJ mol^{-1} for furfural degradation in a study of autocatalytic xylan conversion in the temperature range of 150–190 °C.[54] Similar activation energies for xylose conversion were also reported by Chen *et al.* in the range of 110–127 kJ mol^{-1}.[55] Slight differences can be observed when comparing different kinetic studies due to different reaction temperatures and conditions.

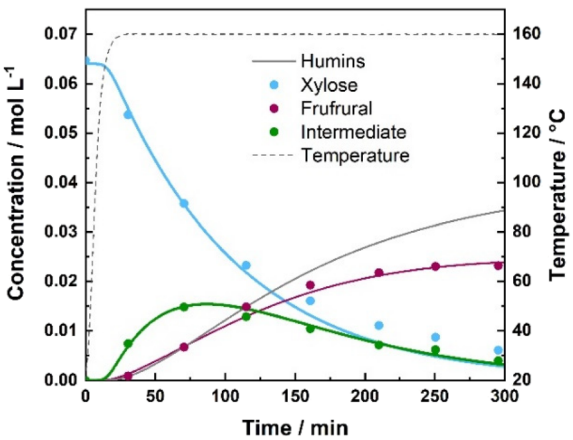

Fig. 3 The product distribution as a function of the time for xylose dehydration reaction in aqueous media with the H-BEA zeolite at 160 °C, where symbols represent experimental points and lines corresponds to model values • xylose, • intermediate • furfural, – humins., ---- temperature.

Kinetics of xylose dehydration over the H-BEA catalyst

As explained above, due to the introduction of strong Lewis acidity, the conversion of xylose proceeded *via* isomerization. The isomerization step itself was found to be favourable for the dehydration of xylose to furfural due to the lower energetic barrier required for the reaction to proceed.[52] This consequently resulted in higher furfural yields at lower operating temperatures, which was especially pronounced at the reaction temperatures of 145 °C and 160 °C.

Notably, the highest operating temperature of 190 °C did not result in an overall improved furfural yield (41 mol%), although the reported yield was achieved at a significantly shorter reaction time (2 h). Increased temperature and the addition of the H-BEA zeolite also highly influenced the xylose conversion and resulted in nearly 100 mol% after 2 h. The concentration profiles of identified products, intermediates and substrates are given in Fig. 3 and ESI Fig. 14.† Based on the calculated kinetic parameters we can notice a significant decrease in the values of E_a, together with an increase of the reaction rate constants of direct xylose dehydration to furfural (k_{X1}) as well as both xylose (k_{X3}) and furfural degradation (k_{X2}) to side products. A reversible isomerization step, promoted by the zeolite's Lewis acidity, proceeds with a reaction rate constant of k_{X4} = 8.4 × 10^{-1} min^{-1} and k_{X7} = 6.97 × 10^{-6} min^{-1}. According to the calculated kinetic parameters, the formed intermediates also tend to be highly reactive, undergoing dehydration to furfural and conversion to degradation products with the highest calculated reaction rate constant of (k_{X5}) 6.4 × 10^{-1} min^{-1} and (k_{X6}) 9.7 × 10^{-1} min^{-1}, respectively. Ferreira *et al.* studied xylose conversion of xylose in aqueous media in the presence of the nanocrystalline beta zeolite at 170 °C. Correspondingly, they demonstrated the highest reaction rate constant for the formation of intermediates from xylose and their dehydration towards furfural and degradation products.[33] Comparing the activation energies, a study conducted by Iglesias *et al.* addressed xylose dehydration over different solid acid catalysts including H-BEA in alcohol media, where they reported the lowest E_a for the degradation of furfural towards degradation products.[56] Similarly, Choudhary *et al.* found

xylose isomerization over Sn-BEA to be favourable for the conversion of xylose to furfural due to a lower energetic barrier required for the reaction to proceed, consequently resulting in higher furfural yield at lower operating temperatures.[36]

Mechanism of glucose/fructose dehydration

Mechanism 3 describes homogeneous dehydration of both glucose and fructose depending on the selection of the starting feedstock. In our study, the results obtained from experiments conducted under hydrothermal treatment conditions demonstrated considerable glucose–fructose isomerization. Therefore, the reaction Mechanism 3, depicted in Fig. 4, includes both direct glucose dehydration (k_{HG7}) into 5-HMF, and reversible glucose isomerization towards fructose (k_{HG4} and k_{HG2}), followed by the dehydration of fructose to 5-HMF (k_{HG1}). Similarly, compared to xylose dehydration, reactions preformed with glucose and fructose resulted in the fragmentation and polymerization of sugar (fructose (k_{HG5}) and glucose (k_{HG6})) and 5-HMF (k_{HG3}) molecules. To confirm the origin of humins, 5-HMF degradation was experimentally investigated in the absence of H-BEA at three different temperatures 130 °C, 160 °C and 190 °C (ESI Fig. 8†). Glucose derived insoluble humins were comparable to xylose derived humins according to SEC analysis, indicating larger molecular species ranging between 150 Da and 2000 Da (ESI, Fig. 7†). The addition of the H-BEA zeolite significantly altered the reaction pathway of glucose/fructose and resulted in newly detected products (levulinic and formic acid). Therefore, the reaction mechanism for glucose dehydration over the selected solid acid catalyst (H-BEA) was modified accordingly (Fig. 4). Due to the unstable nature of 5-HMF, the use of the H-BEA zeolite resulted in its rehydration to levulinic and formic acids. Furthermore, the formed organic acids were not detected in an equimolar ratio indicating towards an additional source of formic acid formation, as levulinic acid has been proved to be stable in this specific temperature range (ESI Fig. 13†). According to the literature, an alternative pathway of humin formation from fructose was suggested to be possible which included simultaneous fructose degradation to humins and formic acid.[30,35,57–59] The proposed reaction scheme of fructose/glucose dehydration over the H-BEA zeolite consequently consists of 8 different reaction steps where k_{G1} is represents fructose dehydration and k_{G7} describes direct glucose dehydration to HMF. Rehydration of HMF to formic and levulinic acid is described by k_{G8}. Steps k_{G2} and k_{G4} represent reversible fructose–glucose and glucose–fructose isomerization reactions, while the reaction rate constants k_{G3}, k_{G5}, and k_{G6} describe 5-HMF, fructose and glucose derived humin formation,

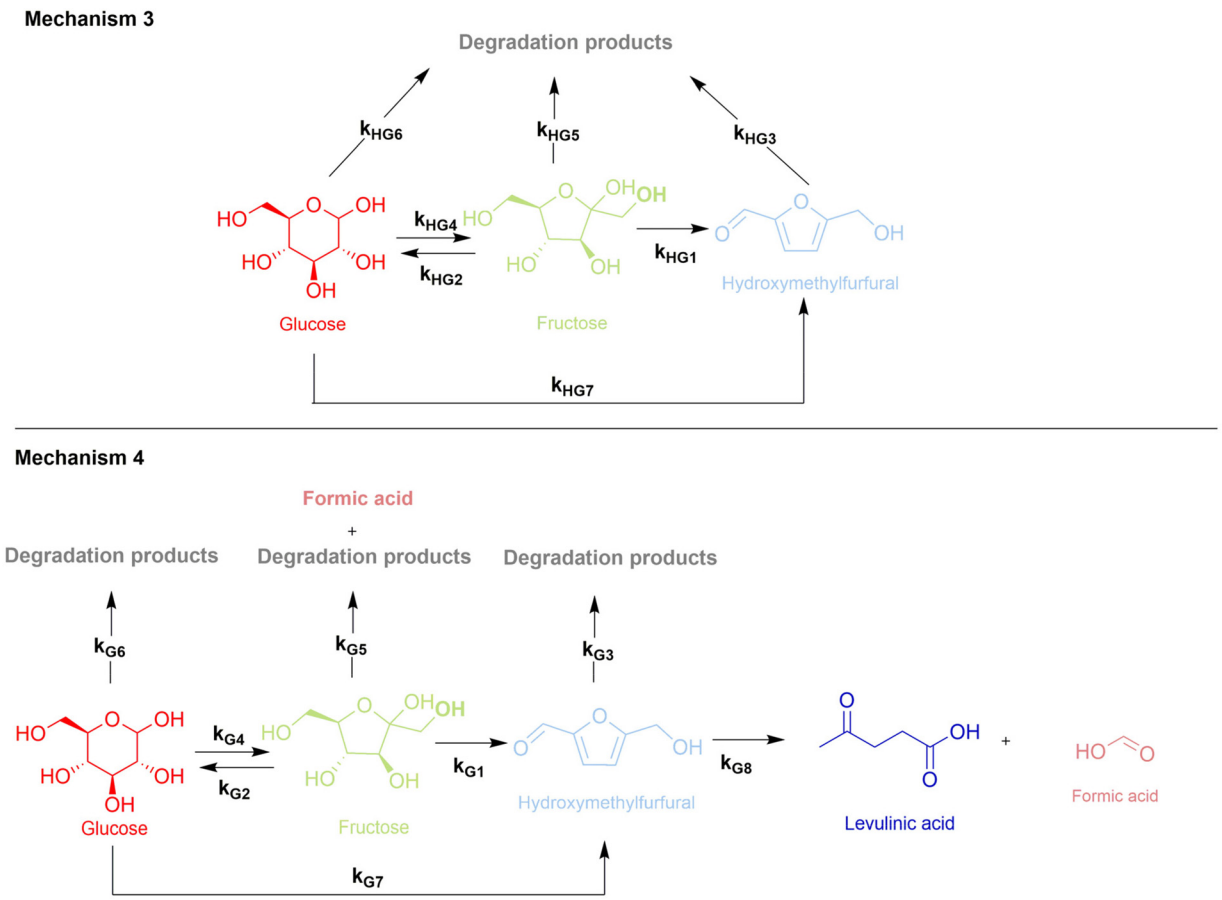

Fig. 4 Homogeneously (mechanism 3) and heterogeneously (mechanism 4) catalysed dehydration of glucose and fructose.

respectively. Fructose-derived humin formation (k_{G5}) involves fructose degradation to degradation products as well as formic acid due to the stoichiometric excess of the detected concentration of formic acid.[37,60] The defined and described reaction network of glucose/fructose conversion (mechanism 4) is in accordance with kinetic models and reaction mechanisms developed by Tang and Swift *et al.* for glucose/fructose dehydration.[37,61] Considering the significant importance of the selected catalyst and reaction solvent system, Yang *et al.* demonstrated the role of Brønsted acidity on glucose dehydration into 5-HMF.[62] Dehydration in the presence solely of a Brønsted acid catalyst proceeds predominantly through the cyclic pathway with limited glucose–fructose isomerization. The glucose isomerization step is principally more pronounced with Lewis acid catalysts due to an induced intramolecular hydride shift.[63] Additionally, isomerization can be facilitated by a Brønsted base *via* the deprotonation of a glucose molecule, acting synergistically and enabling easier Lewis acid catalysed hydride shift.[64] Furthermore, both sugars glucose and fructose have the ability to dehydrate directly into 5-HMF.[28,57,65] Therefore, the developed mechanisms propose that both fructose and glucose as well as 5-HMF can undergo decomposition into degradation products.[38,41,57]

Kinetics of glucose and fructose dehydration in HLW

In addition to xylose, the kinetics of glucose and fructose dehydration was studied for the production of value added chemicals. Reactions conducted with fructose as a starting substrate under hydrothermal conditions demonstrated the trend of increased fructose conversion as the reaction temperature increased, reaching almost 100 mol% at the temperature of 175 °C with a maximum 5-HMF yield of 52 mol% (at 175 °C and 156 min). When the temperature was increased to 190 °C, a slightly lower 49 mol% was achieved in 75 min with a fructose conversion of 84 mol%. As the reaction proceeded, almost 100 mol% fructose conversion was reached within the next sampling time (120 min); however, the 5-HMF yield started steadily decreasing.

Although glucose as a substrate followed a similar trend of increased conversion at the elevated temperature, the highest conversion achieved (86 mol%) was significantly lower in comparison with the conversion of fructose. The maximum yield of 5-HMF recorded with glucose as the starting substrate in the absence of a catalyst appeared to be 33 mol% (at 190 °C and 215 min). The reasoning lies in different reactivities of ketoses and aldoses, where ketoses were found to be convertible more easily with higher selectivity due to the thermodynamically more favourable first step of protonation.[66] The concentrations of substrates, intermediates and products are depicted as a function of time at the temperature of 160 °C in Fig. 5. The influence of temperature on the product distribution for all tested temperatures is presented in ESI Fig. 10 and 11.†

The calculated kinetics parameters revealed 5 times faster dehydration of fructose to 5-HMF (k_{HG1}), compared to direct glucose dehydration (k_{HG7}). Glucose degradation was found to

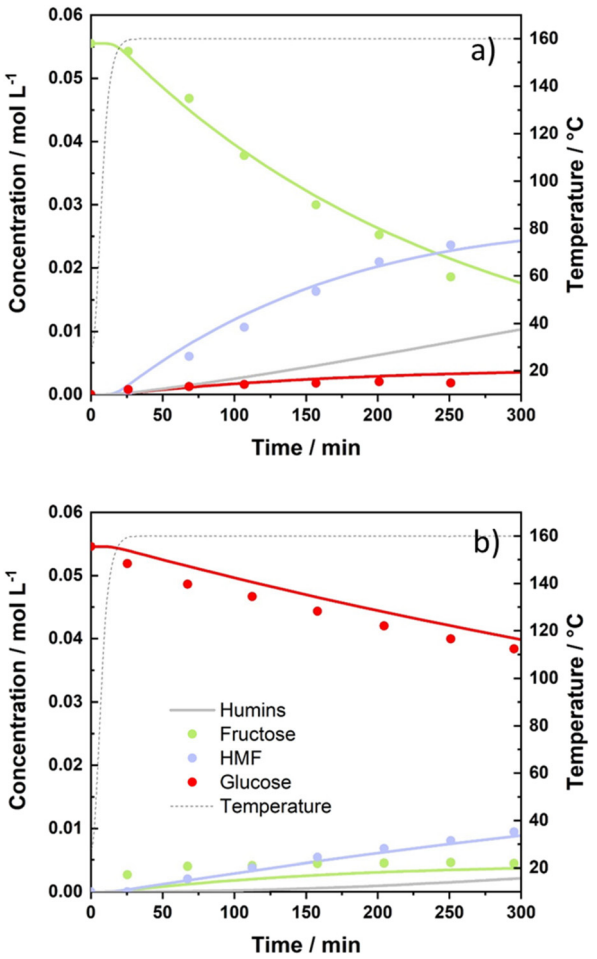

Fig. 5 Product distribution as a function of the time for (a) fructose and (b) glucose dehydration reaction in aqueous media without H-BEA at 160 °C, where symbols represent experimental points and lines corresponds to model values ● fructose, ● 5-HMF, ● glucose, – humins, ----- temperature.

be almost negligible with (k_{HG6}) < 1.6×10^{-6} min^{-1}. However, the conversion of fructose to humins (k_{HG5}) proceeded considerably faster despite being 3 times slower than the degradation of 5-HMF (k_{HG3}). Based on the established kinetic model, relatively high activation energies of 139 kJ mol^{-1} and 120 kJ mol^{-1} were calculated for the dehydration of fructose to 5-HMF and its conversion to degradation products, respectively. The data therefore imply greater temperature dependency for fructose conversion towards 5-HMF as well as other degradation products compared to glucose. The calculated kinetic parameters of homogeneously catalysed glucose and fructose are presented below in Table 3. Although direct comparisons of kinetic parameters obtained from the literature are difficult due to varying reaction conditions and kinetic models, our kinetic parameters correlate well with those of others for glucose and/or fructose dehydration in aqueous environments.[30,35] Activation energies often reported for homogeneously (HCl or H_2SO_4) catalysed glucose dehydration to 5-HMF usually ranges between 108 and 160 kJ mol^{-1}, while

activation energies for the dehydration of fructose to 5-HMF are typically estimated to be between 88 and 161 kJ mol^{-1}.[30,31,35,38,57–59,67–70] Furthermore, our calculated E_a values for fructose and 5-HMF degradation are in accordance with the study conducted by Li *et al.* of fructose decomposition in the absence of a catalyst in high temperature liquid water.[69]

Kinetics of glucose and fructose dehydration over the H-BEA catalyst

The addition of the zeolite highly impacted fructose and glucose dehydration reactions and its final product distribution. The addition of the H-BEA zeolite substantially lowered the highest 5-HMF yield achieved solely by hydrothermal treatment of both glucose and fructose. Therefore, glucose dehydration resulted in merely 10 mol% of 5-HMF, attained at 190 °C and 75 min, whereas fructose dehydration led to 14 mol% 5-HMF yield at 175 °C after 73 min. Increasing the reaction temperature for H-BEA catalysed fructose conversion to 190 °C resulted in a lower 5-HMF yield (12 mol%), which started decreasing after 75 min. This phenomenon can be explained by the facilitation of some reaction steps such as rehydration and humin formation, respectively. As the reaction proceeds, 5-HMF tends to rehydrate further into levulinic and formic acid. When starting from glucose, the highest yield of levulinic acid (26 mol%) was attained at 190 °C and 300 min. Likewise, Ramli *et al.* and Wei *et al.* obtained similar yields of LA with unmodified HY and HZSM zeolites in aqueous environments.[32,71,72] As fructose was introduced as the starting substrate, the dehydration reaction yielded considerably higher amounts of LA at lower operating temperatures, achieving 28 mol%, at 175 °C. As the temperature was increased to 190 °C, the LA yield obtained by fructose dehydration over the H-BEA zeolite reached a maximum of 30 mol% considerably faster.

Product distribution during heterogeneously catalysed glucose/fructose dehydration at 160 °C is presented in Fig. 6, whereas the concentration profiles at other tested temperatures are shown in ESI Fig. 15 and 16.† Elevated temperatures subsequently lead to increased amounts of LA. However, as the temperature was increased to 190 °C, reactions of degradation overruled the process and compromised the 5-HMF yield in particular. In the reaction with the H-BEA zeolite, 5-HMF appears as an intermediate and its concentration starts steadily decreasing over time, especially above 175 °C. With the increase in temperature and H-BEA zeolite addition, the glucose–fructose isomerization reaction became more pronounced and higher fructose/glucose concentrations were detected. Compared to the homogeneous reaction, H-BEA displays strong activity resulting in almost 100% glucose and fructose conversion at 190 °C, while with regard to selectivity, catalyst addition presented higher selectivity towards levulinic acid compared to 5-HMF. Therefore, it can be concluded that the addition of the H-BEA zeolite can be favourable for glucose/fructose conversion towards LA, while the addition of this specific catalyst does not preserve 5-HMF selectivity due to the facilitated reactions of 5-HMF rehydration and humin formation, respectively. The latter can be additionally demonstrated by calculated kinetic parameters where (k_{G8}) the reaction rate constant of rehydration was the highest, followed by the reaction rate constant of 5-HMF derived humin formation (k_{G3}). The reactions of isomerization and 5-HMF derived humin formation were the most influenced by the increase in temperature, with the highest activation energies of 136 kJ mol^{-1}, 151 kJ mol^{-1} and 140 kJ mol^{-1}, respectively. Generally, activation energies were significantly lowered in the presence of H-BEA, especially for dehydration, although E_a was also undesirably lowered towards humin formation. As expected, the H-BEA zeolite strongly facilitated the glucose–fructose isomerization reaction, moving the equilibrium slightly towards fructose formation ($k_{G4} > k_{G2}$), which favourably affected the overall catalyst efficiency for 5-HMF and LA production. Lourvanij *et al.* presented similar conclusions in one of the first kinetic studies on glucose dehydration over a HY-zeolite, where isomerization, 5-HMF rehydration and degradation steps tend to proceed much faster in comparison with the rest

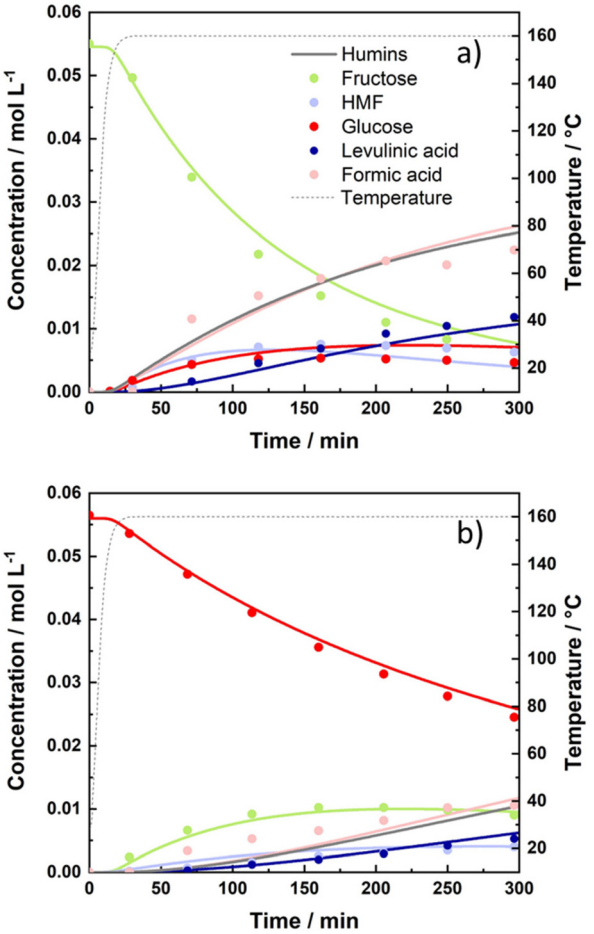

Fig. 6 Product distribution as a function of the time for (a) fructose and (b) glucose dehydration reaction in aqueous media with the H-BEA zeolite at 160 °C, where symbols represent experimental points and lines corresponds to model values • fructose, • 5-HMF, • glucose, • levulinic acid, • formic acid, – degradation products, ----- temperature.

of the reactions.[28] Our calculated activation energies of glucose/fructose isomerization and 5-HMF derived humin correlate well with the study conducted by Swift *et al.*, who similarly studied saccharide conversion over H-BEA.[37]

Comparison of xylose glucose and fructose dehydration kinetics under hydrothermal reaction conditions

According to the activation energies and experimental data, the dehydration of all three saccharides demonstrated to be significantly influenced by the increase in temperature. This impact was the most pronounced with fructose dehydration, followed by xylose, while the direct dehydration of glucose to 5-HMF was not affected as prominently. A similar trend comparing xylose and glucose conversion was observed by Dussan *et al.*[70] Notably, xylose degradation into humins was shown to have the highest E_a (213 kJ mol^{-1}), followed by fructose degradation (120 kJ mol^{-1}), and glucose-derived humin formation was the lowest (78 kJ mol^{-1}). Therefore, glucose degradation towards humins was found to be the least temperature dependent, comparable to what was reported by dos Santos Rocha *et al.* and Dussan *et al.*[70,73] Likewise, a specific trend was observed comparing the reaction rate constants. The reaction rate constant of fructose dehydration (k_{HG1}) was almost three times faster relative to xylose (k_{HX1}), while direct glucose dehydration (k_{HG7}) appeared to be nearly 2 times slower compared to xylose (k_{HX1}). In correspondence to dos Santos Rocha *et al.*, the degradation of furfural had a higher activation energy compared to the degradation of 5-HMF, suggesting that its degradation would be more pronounced at increased temperatures.[73] However, a notably higher E_a of furfural degradation was also accompanied by a lower reaction rate constant, demonstrating its slower degradation.

Nevertheless, the conversion and yields/selectivity of the dehydration reactions all of the three selected saccharides, xylose, glucose and fructose, towards the desired products (5-HMF and furfural) differed significantly. Fructose reached the highest conversion at most of the reaction temperatures, with nearly 100 mol% already at 175 °C. Conversion of xylose resulted in nearly 97 mol%, while the highest attained glucose conversion was significantly lower with 86 mol% at 190 °C. Similarly, the dehydration of fructose resulted in 52 mol% of 5-HMF yield, followed by the dehydration of xylose yielding 45 mol% of furfural, while 33 mol% yield of 5-HMF was achieved when using glucose as a starting substrate, as depicted in Fig. 7. Generally, results agree well with the literature which imply greater reactivity of saccharides in the ketose form (fructose) in comparison with aldoses (glucose and xylose), while among aldoses, C5 sugars/pentoses resulted in higher conversion at elevated temperatures.[66,74–76]

Comparison of xylose and glucose dehydration kinetics in the presence of a zeolite as the solid acid catalyst

The addition of the H-BEA zeolite had a profound effect on the conversion of all studied saccharides, namely xylose, glucose and fructose, respectively. Conversion of all three saccharides was significantly increased, reaching almost 100 mol% for xylose and fructose at the temperature of 175 °C, although when the reaction temperature was increased further, all three saccharides resulted in 100 mol% conversion, as seen in Fig. 8. Xylose dehydration over the H-BEA zeolite resulted in higher yields at lower operational temperatures, whereas the temperatures of 175 °C and 190 °C yielded 38 mol% and 42 mol% in a significantly shorter time compared to without the added catalyst under the same reaction conditions.

Comparing xylose, fructose and glucose dehydration catalysed by the H-BEA zeolite, 5-HMF appeared much less stable and was easily converted further towards levulinic and formic acid. Therefore, 5-HMF yields were not improved by the introduction of the H-BEA zeolite. This was additionally validated by the lower reaction rate constant of furfural derived humin formation in comparison with 5-HMF degradation. On the other hand, dehydration of both C6 saccharides resulted in a significant amount of levulinic acid. Comparing the calculated kinetic parameters, the direct saccharide conversion towards

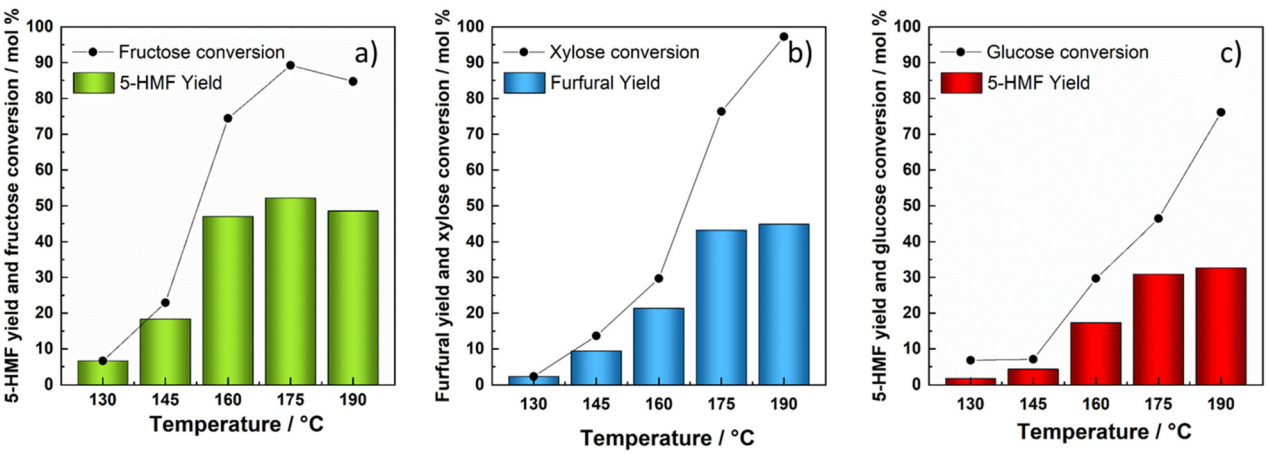

Fig. 7 The maximal conversion and (5-HMF and furfural) yield of fructose (a), xylose (b) and glucose (c) at five different temperatures 130, 145, 160, 175 and 190 °C, under hydrothermal conditions without catalyst.

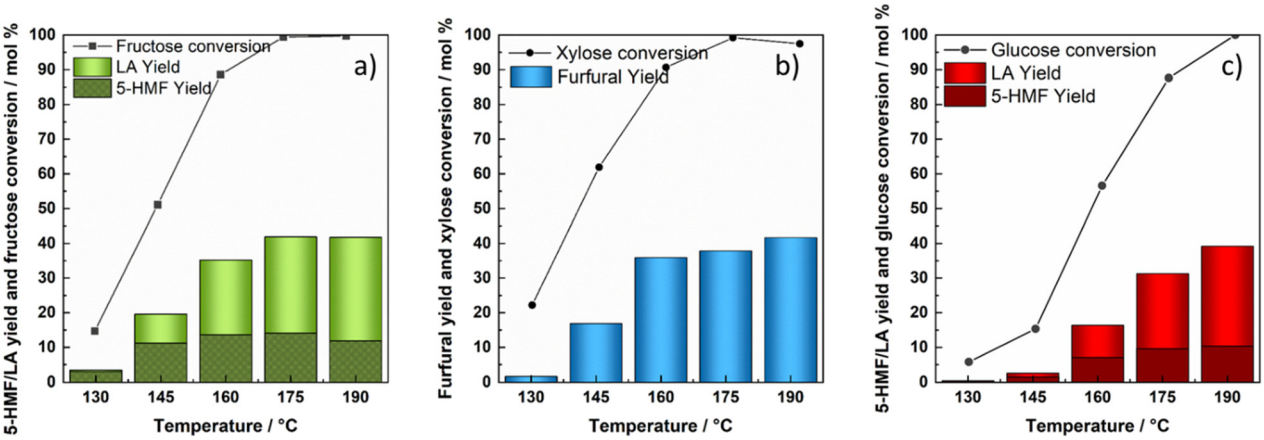

Fig. 8 The maximal conversion and (5-HMF/LA and furfural) yield of fructose (a), xylose (b) and glucose (c) at five different temperatures 130, 145, 160, 175 and 190 °C, under hydrothermal conditions with the H-BEA zeolite.

furanics (furfural and 5-HMF) proceeded much slower, while the reaction rate constants of isomerization for both xylose and glucose were significantly higher. Intermediates (fructose and lyxose/xylulose) resulted in a relatively high calculated activation energy. In contrast, the degradation of glucose and xylose towards humins resulted in a low E_a. Comparing the reactivity of the three different saccharides, xylose, glucose and fructose, with and without the H-BEA zeolite under hydrothermal reaction conditions followed the same trend in saccharide reactivity (fructose > xylose > glucose). Similar findings were reported by Cinlar *et al.* comparing the conversion of monosaccharides in the presence of homogeneous Brønsted acid catalysts including HCl, H_2SO_4, H_3PO_4, maleic and 1-propane sulfonic acid.[77]

Optimization of saccharide dehydration

Based on these established kinetic models, we predicted the optimal process conditions (time and temperature) to attain maximum yields of desirable compounds, 5-HMF and LA. According to the results of optimization, the highest 5-HMF yield (60 mol%) was expected to be achieved by homogeneous fructose dehydration at the maximum operating temperature (223 °C) and the shortest reaction time (30 min). As homogeneously catalysed fructose dehydration has the highest E_a, as well as the highest reaction rate constant, the reaction will dominate and proceed the fastest at higher temperatures. Additionally, in order to preserve the highest yield of 5-HMF and avoid its degradation, the reaction time should be shortened accordingly. This was subsequently experimentally confirmed with fructose dehydration in HLW in the absence of a catalyst, as shown in Fig. 9a. The highest yield of 5-HMF (52 mol%) was achieved experimentally in 34 min and at the temperature of 234 °C. Overall, validation tests were in very good agreement with the predicted values. The difference in the predicted *vs.* experimental values was anticipated to be due to two main reasons: (i) heat transfer limitations during the ramp up in the batch reactor system, and (ii) the validation experiments were conducted outside the studied temperature range. From the obtained results, it can be concluded that the ideal system for 5-HMF production would be a continuous setup, which allows short residence times and high operating

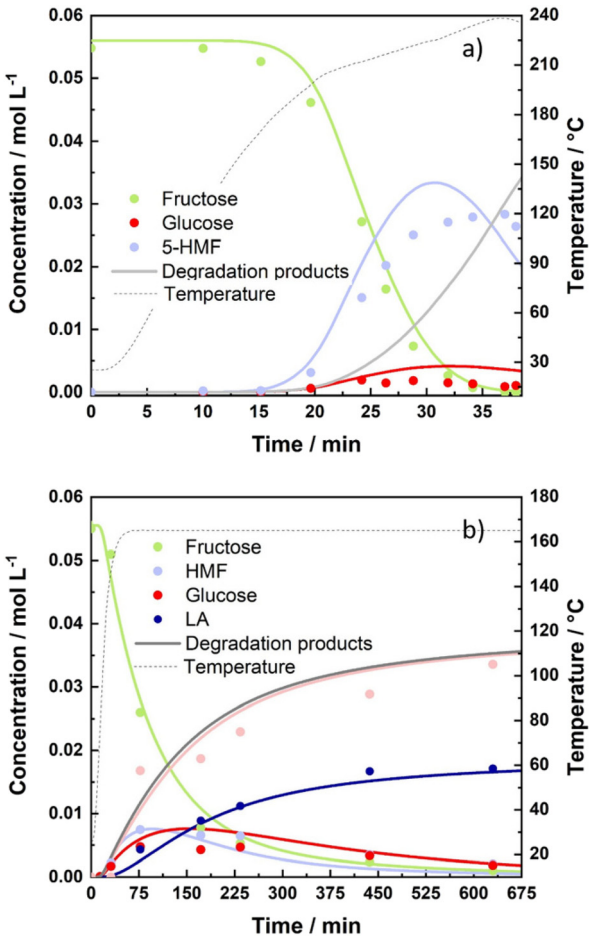

Fig. 9 Validation experiments of (a) homogeneous fructose dehydration and (b) H-BEA catalysed fructose conversion under the predicted optimal conditions.

temperatures. In contrast, the optimal process conditions for the production of levulinic acid specifically require the presence of the H-BEA zeolite, longer reaction times and moderate temperatures. Based on the established kinetic model, the predicted highest yield of LA was 31 mol% at 10 h and 165 °C. The validation experiment resulted in the highest achieved LA yield of 30.5 mol%, as shown in Fig. 9b. Although the reaction of 5-HMF rehydration proceeds the fastest, the dehydration reaction appears to be the rate limiting step. Therefore, the optimal process conditions for the production of LA in a batch regime would require relatively long reaction times. Furthermore, moderate temperature of 165 °C is required due to the relatively high activation energies of reactions leading to saccharide/5-HMF degradation to humins compared to the low E_a for the rehydration reaction.

The obtained results of optimal process conditions can be directly compared to the commercial Biofine process.[22] The process involves the hydrolysis of biomass towards monosaccharides, which are then further converted to levulinic acid, formic acid and furfural. High concentrations of 5-HMF (an intermediate) are achieved during the process with a high operating temperature of 210–220 °C and a very short residence time, while further conversion to levulinic acid requires rather moderate process conditions (lower temperature and longer residence times).

Conclusion

In this work, we studied the conversion of three of the most prominent biomass-derived saccharides (xylose, fructose, and glucose). Dehydration reactions were conducted under hydrothermal conditions (130–190 °C) in the absence and presence of the H-BEA zeolite, selected as a commercially available heterogeneous acid catalyst. Reactions performed without the catalyst in aqueous media demonstrated substantial saccharide conversion with significant amounts of 5-HMF and furfural, confirming the catalytic activity of subcritical water. Therefore, we developed two parallel kinetic models; the first model was related to the catalytic activity occurring solely by hydrothermal treatment. The model was later expanded to a kinetic model of H-BEA zeolite catalysed dehydration which considers reactions on the catalyst surface, adsorption and desorption rates onto acid sites, and thermodynamic influences.

The modelled values are in great agreement with the experimental results, elucidating the complex reaction mechanisms of saccharide conversion and serving as a basis for process optimization and future rational catalyst design. The H-BEA zeolite was found to improve yields and/or shorten the time of the reaction to achieve maximum furfural yields. The addition of the catalyst substantially influenced glucose and fructose conversion and resulted in a lower 5-HMF yield. However, it was shown to be significantly beneficial for the production of LA. Additionally, kinetic analysis demonstrated that H-BEA lowers the energy barrier (E_a) of xylose and glucose/fructose dehydration to furfural and 5-HMF/LA. The catalyst proved to have high activity, but it would require additional tuning of its acidity in order to achieve higher selectivity towards the desirable products. The developed kinetic model and calculated kinetic parameters allowed further optimization of process conditions in order to maximize the yields of 5-HMF and LA. The predicted conditions have been experimentally validated and demonstrated excellent correlation with the forecasted results. The homogeneously catalysed fructose dehydration reaction, with a relatively high E_a and reaction rate constant for direct fructose dehydration, yielded in the maximal concentration of 5-HMF in a very short residual time (34 min) and at a relatively high reaction temperature (234 °C). In contrast, the optimal conditions for maximal yield of LA proved to be attained during the H-BEA catalysed reaction, at a moderate temperature (165 °C) and longer reaction times (10 h) due to the lower E_a calculated for the rehydration of 5-HMF. Overall, the results under hydrothermal treatment in the presence and absence of the catalysts resulted in greater conversion of saccharides in ketose form (fructose) in comparison with aldoses (glucose and xylose). Furthermore, the dehydration of aldopentoses (xylose) leads to higher conversions compared to aldo-hexoses (glucose), particularly at increased temperatures. Future work will focus on catalyst design and process optimization for each of the bio-based value-added compound with an emphasis on curtailing humin formation as an undesirable side product.

Conflicts of interest

There are no conflicts to declare.

Acknowledgements

The authors would like to appreciatively acknowledge the financial support of the EU Framework Program for Research and Innovation Horizon 2020 under Grant agreement no. 887226 (BioSPRINT) and the Slovenian Research Agency (Program P2-0152 and research project J2-2492). Dr Huš and Mr Harth are acknowledged for fruitful discussion regarding the dissemination aspects of this work.

References

1 Y. Liu, Y. Tang, H. Gao, W. Zhang, Y. Jiang, F. Xin and M. Jiang, *Molecules*, 2021, **26**, 5411.
2 M. Lang and H. Li, *ChemSusChem*, 2022, **15**, e202101531.
3 D. M. Alonso, J. Q. Bond and J. A. Dumesic, *Green Chem.*, 2010, **12**, 1493–1513.
4 R. J. Van Putten, J. C. Van Der Waal, E. De Jong, C. B. Rasrendra, H. J. Heeres and J. G. De Vries, *Chem. Rev.*, 2013, **113**, 1499–1597.
5 B. Pomeroy, M. Grilc, S. Gyergyek and B. Likozar, *Chem. Eng. J.*, 2021, **412**, 127553.

6 K. I. Galkin and V. P. Ananikov, *ChemSusChem*, 2019, **12**, 2976–2982.
7 K. Kohli, R. Prajapati and B. K. Sharma, *Energies*, 2019, **12**, 233.
8 X. Li, P. Jia and T. Wang, *ACS Catal.*, 2016, **6**, 7621–7640.
9 R. Šivec, M. Grilc, M. Huš and B. Likozar, *Ind. Eng. Chem. Res.*, 2019, **58**, 16018–16032.
10 B. Pomeroy, M. Grilc and B. Likozar, *Green Chem.*, 2021, **23**, 7996–8002.
11 A. Morone, M. Apte and R. A. Pandey, *Renewable Sustainable Energy Rev.*, 2015, **51**, 548–565.
12 Y. Zhao, K. Lu, H. Xu, L. Zhu and S. Wang, *Renewable Sustainable Energy Rev.*, 2021, **139**, 110706.
13 H. Wang, C. Zhu, D. Li, Q. Liu, J. Tan, C. Wang, C. Cai and L. Ma, *Renewable Sustainable Energy Rev.*, 2019, **103**, 227–247.
14 T. Wang, M. W. Nolte and B. H. Shanks, *Green Chem.*, 2014, **16**, 548–572.
15 I. Van Zandvoort, Y. Wang, C. B. Rasrendra, E. R. H. Van Eck, P. C. A. Bruijnincx, H. J. Heeres and B. M. Weckhuysen, *ChemSusChem*, 2013, **6**, 1745–1758.
16 G. Tsilomelekis, M. J. Orella, Z. Lin, Z. Cheng, W. Zheng, V. Nikolakis and D. G. Vlachos, *Green Chem.*, 2016, **18**, 1983–1993.
17 L. Zhu, X. Fu, Y. Hu and C. Hu, *ChemSusChem*, 2020, **13**, 4812–4832.
18 B. Danon, G. Marcotullio and W. De Jong, *Green Chem.*, 2014, **16**, 39–54.
19 Z. Cheng, J. L. Everhart, G. Tsilomelekis, V. Nikolakis, B. Saha and D. G. Vlachos, *Green Chem.*, 2018, **20**, 997–1006.
20 M. Marzo, A. Gervasini and P. Carniti, *Catal. Today*, 2012, **192**, 89–95.
21 I. V. Sumerskii, S. M. Krutov and M. Y. Zarubin, *Russ. J. Appl. Chem.*, 2010, **83**, 320–327.
22 D. J. Hayes, S. Fitzpatrick, M. H. B. Hayes and J. R. H. Ross, in *Biorefineries - Industrial Processes and Products*, 2006, vol. 1, pp. 139–164.
23 P. Ganji, *Biomass Convers. Biorefin.*, 2020, **10**, 823–830.
24 X. Zhang, K. Wilson and A. F. Lee, *Chem. Rev.*, 2016, **116**, 12328–12368.
25 L. Hu, Z. Wu, Y. Jiang, X. Wang, A. He, J. Song, J. Xu, S. Zhou, Y. Zhao and J. Xu, *Renewable Sustainable Energy Rev.*, 2020, **134**, 110317.
26 J. Jiang, W. Ding and H. Li, *Renewable Energy*, 2021, **179**, 1262–1270.
27 R. Zong, H. Li, W. T. Ding and H. Huang, *ACS Sustainable Chem. Eng.*, 2021, **9**, 9891–9902.
28 K. Lourvanij and G. L. Rorrer, *J. Chem. Technol. Biotechnol.*, 1997, **69**, 35–44.
29 R. O'Neill, M. N. Ahmad, L. Vanoye and F. Aiouache, *Ind. Eng. Chem. Res.*, 2009, **48**, 4300–4306.
30 B. A. Fachri, R. M. Abdilla, H. H. V. De Bovenkamp, C. B. Rasrendra and H. J. Heeres, *ACS Sustainable Chem. Eng.*, 2015, **3**, 3024–3034.
31 Q. Jing and X. Lü, *Chin. J. Chem. Eng.*, 2008, **16**, 890–894.
32 W. Wei and S. Wu, *Fuel*, 2018, **225**, 311–321.
33 L. R. Ferreira, S. Lima, P. Neves, M. M. Antunes, S. M. Rocha, M. Pillinger, I. Portugal and A. A. Valente, *Chem. Eng. J.*, 2013, **215–216**, 772–783.
34 Q. Jing, X. Lu and L. Yuan, *Chem. React. Eng. Technol.*, 2006, **22**, 472–475.
35 B. Girisuta, L. P. B. M. Janssen and H. J. Heeres, *Chem. Eng. Res. Des.*, 2006, **84**, 339–349.
36 V. Choudhary, A. B. Pinar, S. I. Sandler, D. G. Vlachos and R. F. Lobo, *ACS Catal.*, 2011, **1**, 1724–1728.
37 T. D. Swift, H. Nguyen, Z. Erdman, J. S. Kruger, V. Nikolakis and D. G. Vlachos, *J. Catal.*, 2016, **333**, 149–161.
38 W. Guo, Z. Zhang, J. Hacking, H. J. Heeres and J. Yue, *Chem. Eng. J.*, 2021, **409**, 128182.
39 R. Šivec, M. Huš, B. Likozar and M. Grilc, *Chem. Eng. J.*, 2022, **436**, 32–40.
40 A. Kojčinović, Ž. Kovačič, M. Huš, B. Likozar and M. Grilc, *Appl. Surf. Sci.*, 2021, **543**, 148836.
41 C. E. Bounoukta, C. Megías-Sayago, F. Ammari, S. Ivanova, A. Monzon, M. A. Centeno and J. A. Odriozola, *Appl. Catal., B*, 2021, **286**, 119938.
42 A. Kostyniuk, D. Bajec and B. Likozar, *Appl. Catal., A*, 2021, **612**, 118004.
43 A. Palčić and V. Valtchev, *Appl. Catal., A*, 2020, **606**, 117795.
44 Z. Wang, Y. Jiang, O. Lafon, J. Trébosc, K. D. Kim, C. Stampfl, A. Baiker, J. P. Amoureux and J. Huang, *Nat. Commun.*, 2016, **7**, 1–5.
45 H. Fujita, T. Kanougi and T. Atoguchi, *Appl. Catal., A*, 2006, **313**, 160–166.
46 J. S. Kruger, V. Choudhary, V. Nikolakis and D. G. Vlachos, *ACS Catal.*, 2013, **3**, 1279–1291.
47 T. K. Phung and G. Busca, *Appl. Catal., A*, 2015, **504**, 151–157.
48 J. Köchermann, J. Mühlenberg and M. Klemm, *Ind. Eng. Chem. Res.*, 2018, **57**, 14417–14427.
49 Y. Yu and H. Wu, *Ind. Eng. Chem. Res.*, 2011, **50**, 10500–10508.
50 M. Möller, F. Harnisch and U. Schröder, *Biomass Bioenergy*, 2012, **39**, 389–398.
51 D. R. Hua, Y. L. Wu, Y. F. Liu, Y. Chen, M. De Yang, X. N. Lu and J. Li, *Pet. Sci.*, 2016, **13**, 167–172.
52 V. Choudhary, S. I. Sandler and D. G. Vlachos, *ACS Catal.*, 2012, **2**, 2022–2028.
53 V. Choudhary, S. Caratzoulas and D. G. Vlachos, *Carbohydr. Res.*, 2013, **368**, 89–95.
54 D. Nabarlatz, X. Farriol and D. Montané, *Ind. Eng. Chem. Res.*, 2004, **43**, 4124–4131.
55 X. J. Chen, X. Q. Liu, F. L. Xu and X. P. Bai, *Adv. Mater. Res.*, 2012, **450–451**, 710–714.
56 J. Iglesias, J. A. Melero, G. Morales, M. Paniagua and B. Hernández, *ChemCatChem*, 2016, **8**, 2089–2099.
57 D. Garcés, E. Díaz and S. Ordóñez, *Ind. Eng. Chem. Res.*, 2017, **56**, 5221–5230.
58 T. D. Swift, C. Bagia, V. Choudhary, G. Peklaris, V. Nikolakis and D. G. Vlachos, *ACS Catal.*, 2014, **4**, 259–267.
59 F. S. Asghari and H. Yoshida, *Ind. Eng. Chem. Res.*, 2007, **46**, 7703–7710.

60 T. D. Swift, C. Bagia, V. Choudhary, G. Peklaris, V. Nikolakis and D. G. Vlachos, *ACS Catal.*, 2014, **4**, 259–267.
61 J. Tang, L. Zhu, X. Fu, J. Dai, X. Guo and C. Hu, *ACS Catal.*, 2017, **7**, 256–266.
62 L. Yang, G. Tsilomelekis, S. Caratzoulas and D. G. Vlachos, *ChemSusChem*, 2015, **8**, 1334–1341.
63 E. A. Pidko, V. Degirmenci, R. A. Van Santen and E. J. M. Hensen, *Inorg. Chem.*, 2010, **49**, 10081–10091.
64 V. Choudhary, A. B. Pinar, R. F. Lobo, D. G. Vlachos and S. I. Sandler, *ChemSusChem*, 2013, **6**, 2369–2376.
65 C. Wang, L. Zhang, T. Zhou, J. Chen and F. Xu, *Sci. Rep.*, 2017, **7**, 1–9.
66 G. Yang, E. A. Pidko and E. J. M. Hensen, *J. Catal.*, 2012, **295**, 122–132.
67 L. Kupiainen, J. Ahola and J. Tanskanen, *Chem. Eng. Res. Des.*, 2011, **89**, 2706–2713.
68 R. Weingarten, J. Cho, R. Xing, W. C. Conner and G. W. Huber, *ChemSusChem*, 2012, **5**, 1280–1290.
69 Y. Li, X. Lu, L. Yuan and X. Liu, *Biomass Bioenergy*, 2009, **33**, 1182–1187.
70 K. Dussan, B. Girisuta, M. Lopes, J. J. Leahy and M. H. B. Hayes, *ChemSusChem*, 2015, **8**, 1411–1428.
71 N. A. S. Ramli and N. A. S. Amin, *Chem. Eng. J.*, 2016, **283**, 150–159.
72 N. A. S. Ramli and N. A. S. Amin, *Appl. Catal., B*, 2015, **163**, 487–498.
73 M. S. R. dos Santos Rocha, B. Pratto, R. de Sousa, R. M. R. G. Almeida and A. J. G. da Cruz, *Bioresour. Technol.*, 2017, **228**, 176–185.
74 S. Rivas, M. J. González-Muñoz, V. Santos and J. C. Parajó, *Bioresour. Technol.*, 2014, **162**, 192–199.
75 R. J. Van Putten, J. N. M. Soetedjo, E. A. Pidko, J. C. Van Der Waal, E. J. M. Hensen, E. De Jong and H. J. Heeres, *ChemSusChem*, 2013, **6**, 1681–1687.
76 T. Istasse and A. Richel, *RSC Adv.*, 2020, **10**, 23720–23742.
77 B. Cinlar, T. Wang and B. H. Shanks, *Appl. Catal., A*, 2013, **450**, 237–242.